

Experimental and analytical behavior of stiffened angle joints

Peng Wang^{1a}, Jianrong Pan^{*1,2}, Zhan Wang^{1,2b} and Shizhe Chen¹

¹School of Civil Engineering and Transportation, South China University of Technology, Guangzhou 510641, China

²State Key Laboratory of Subtropical Building Science, South China University of Technology, Guangzhou 510641, China

(Received July 11, 2017, Revised September 3, 2017, Accepted September 28, 2017)

Abstract. The application of rib stiffeners is common on steel connections, with regard to the stiffened angle connection, experimental results about the influence of stiffeners under monotonic and cyclic loading are very limited. Consequently, this paper presents the experimental investigation on four types angle connections with or without stiffener under static loading and another four type stiffened angle connections subjected to cyclic loading. The static experimental result showed that the rib stiffener weld in tension zone of the connection greatly enhanced its initial rotational stiffness and flexural strength. While a stiffener was applied to the compression zone of the connection, it had not obvious influences on the initial rotational stiffness, but increased its flexural strength. The moment-rotation curves, skeleton curves, ductility, energy dissipation and rigidity were evaluated under cyclic loading. Stiffened top-and-seat angle connections behaved as semi-rigid and partial strength, and rotation of all stiffened angle connections exceeded 0.04rad. The failure modes between monotonic and cyclic loading test were completely different and indicated certain robustness.

Keywords: steel frame; stiffened angle connections; semi-rigid joints; finite element method

1. Introduction

The earthquake occurred in Northridge (Mahin 1998) and Hyogoken Nanbu (Akiyama 2000) caused severe damage in welded steel moment structures, particularly in the joints of the frame. Since then, researchers have suggested many bolted connections as alternative types, including top-and-seat angle connections with high-strength bolts that are designed to support gravitational loads on the beam ends and are classified as pinned connections according to the AISC-LRFD (1995) specifications. However all currently used connections possess stiffness that falls between ideally pinned and fully rigid; therefore, their design should conform to their actual behavior. In order to investigate the real performance of the connection. A wide range of researches were carried out over the past three decades (Azizinamini and Radziminski 1989, Kukreti and Abolmaali 1999, Garlock *et al.* 2003), these studies have resulted in the code specifications stated in Eurocode 3 Part 1.8 (2005).

In order to strengthen the top-and-seat angle connection, rib stiffeners were considered as an effective method in engineering application, the stiffeners welded in end-plate connection usually possessed higher strength and energy absorption capacities and showed different failure modes compared to the un-stiffened one (Guo *et al.* 2006, Shi *et al.*

2008, Ghassemieh *et al.* 2014). With regard to the top-and-seat angle connections that there are limited studies about stiffened angle joints under monotonic and cyclic loading condition.

Skejjic *et al.* (2014) studied the static characteristics of a stiffened angle connection of a major axis according to Eurocode 3 part 1.8 (2005), all high strength bolts were tightened to a lower level pretension force of approximately 20% of the bolt tension strength, which differs from the Chinese code for design of steel structures (2003). This different pretension led to different connection rotation stiffness and strength (Piluso and Faella 1998, Citipitioglu *et al.* 2002). Reinoso and Loureiro *et al.* (2015) proposed an analytical plate approach for the axial stiffness prediction of stiffened angle cleats. Aydın *et al.* (2015) investigated monotonic loading beam-to-column connections designed with in minor column axes to analyze the influence of angle with and without stiffeners on the behavior of the beam-to-column connections, particularly the deflection of column web strongly influenced the behavior of the connection in minor axes.

As mentioned above. The experiments for steel connection were costly and time consuming, FEM (finite element method) for numerical study as an alternative way has been widely used in steel connection for static and cyclic loading condition. Citipitioglu *et al.* (2002) employed 3D solid element to capture the real mechanical property of the top and seat angles with double web angles connection in monotonic load, the numerical research had consider the contact between steel assembly and pretension force in high-strength bolts. Danesh *et al.* (2007) validated the experimental work of Azizinamini and Radziminski (1989) by ANSYS multi-purpose finite element simulation code. Liu *et al.* (2014) adopted finite element models to

*Corresponding author, Professor

E-mail: ctjrpan@scut.edu.cn

^aPh.D. Student

E-mail: ctjrpan@scut.edu.cn

^bProfessor

E-mail: wangzhan@scut.edu.cn

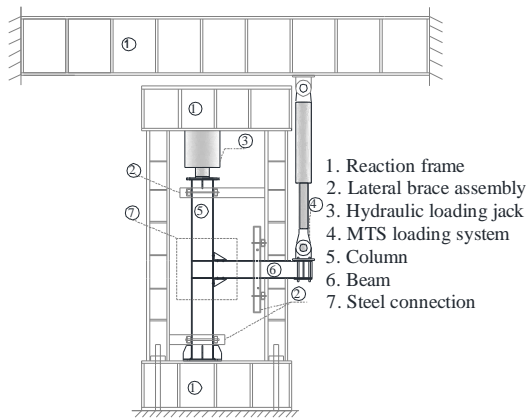


Fig. 1 Test setup

investigate the behavior of open beam-to-tubular column angle connections subjected to different loading conditions. Brunesi *et al.* (2014) simulated the response of partially-restrained bolted beam-to-column under cyclic loads by solid element and simplified FE models based on inelastic force-based fiber element. Abdalla *et al.* (2014) used the software ABAQUS to investigate the shear failure and prying force of top-and-seat angles with double web angles connection. Shiravand and Mahboubi (2016) adopted a pair of stiffened angle in post-tensioned connections for numerical simulation, the FEM result shows that stiffeners help concentrating the more residual deformation in the top-and-seat angles and increase the energy dissipation capacity of the connection.

Therefore, the rib stiffener play a vital role in top-and-seat connections under different loading condition, especially the failure modes, hysteretic behavior and energy absorption are fundamental requirements for seismic design (Feizi *et al.* 2015). This paper discussed an investigation of the entire monotonic and hysteretic behavior of un-stiffened and stiffened top-and-seat angle beam-to-column connections that were subjected to a load applied in the beam tip, and considered the following characteristics: the unstiffened and stiffened angle, the double web angles in the joint, the initial rotational stiffness, plastic flexural resistance, failure mechanism, hysteretic curves, ductility, energy dissipation and rigidity. In this way, a 3D nonlinear finite element model was developed for validating the experiment results and parameter study.

2. Experimental program

2.1 Test detail and setup

Experimental work was conducted at The State Key Laboratory of Subtropical Building Science at the South China University of Technology. The two ends of a column were fixed with a steel assembly and loaded by a vertical hydraulic jack at the top to restrict rotation and displacement as shown in Fig. 1. The beam was connected to the column by a pair of unstiffened or stiffened angle with several high-strength bolts. A lateral brace was set-up to ensure the outside plane stability of the beam during the

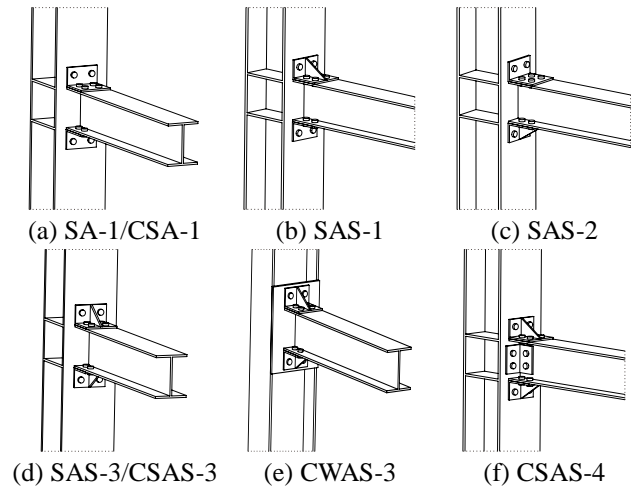


Fig. 2 Specimens for the test

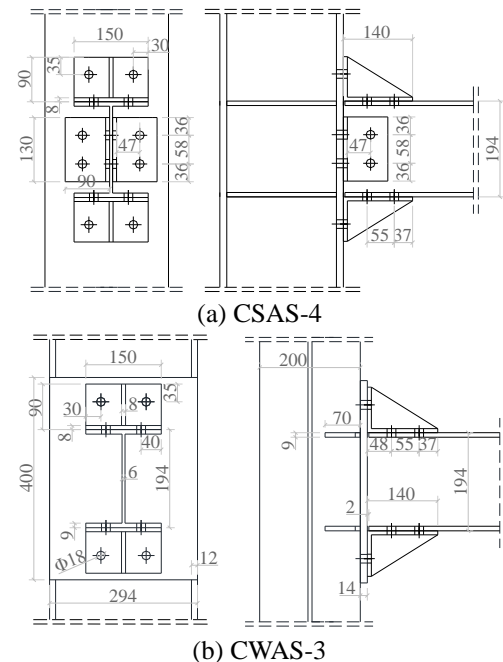


Fig. 3 Geometry configuration of steel specimens

test. One MTS hydraulic jack was linked to the cantilever beam end to impose the displacement history.

Two series of eight bolted top-and-seat angle connections were investigated by experiment in this research. The test setup is shown in Fig. 2. To obtain the real behavior of different types of bolted angle connections during bending, all specimens of angle (L140×90×8 with steel grade Q235), columns (HW250×255×14×14 with steel grade Q345 named column 1; HM294×200×8×12 with steel grade Q235 named column 2) and beams (HM194×150×6×9 with steel grade Q235) were hot rolled steel. All high-strength bolts (M16×70, grade 10.9, a bolt hole diameter was 18 mm) used in the test were tightened with a manual torque wrench to a pretension force of 100 kN that was higher than Skejic's. (2014) test according to Chinese code for design of steel structures (2003). The gap between column and beam was 2 mm. Four specimens had top-and-seat angles in a beam-to-column connection design for

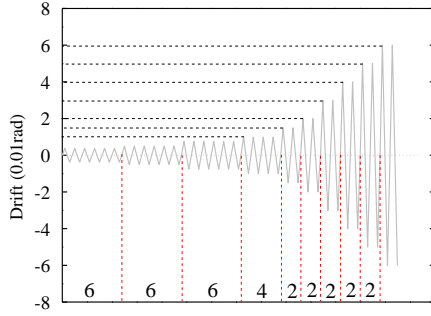


Fig. 4 Loading curve for cyclic test

static loading. The specimen with a rib stiffener welded in top angle was named SAS-1, the seat angle reinforced one was named SAS-2, the specimen SAS-3 was the one that both top angle and seat angle were stiffened, unstiffened one was a control group named SA-1. Another four specimens were design to subject cyclic loading, the name of specimens SA-1 and SAS-3 was add letter C for representing cyclic loading, and CSAS-4 was the stiffened one with double web angles, CWAS was new design for beam connected to the minor axis. The details are illustrated in Figs. 2-3.

2.2 Loading protocol

The testing specimens were mounted to a reaction frame and whole device diagram of experiment setup as shown in Fig. 1, all testing columns was 2 m in length. The distance between the column flange and the actuator loading point was 1m. Thus, when the displacement of beam tip achieved 1.0% a story drift was 10 mm. In the monotonic test, the load was stopped until the connection cracked or the loading devices limit was reached. The cyclic test-piece was loaded according to the SAC Joint Venture (1997) in a relative low speed as shown in Fig. 4.

2.3 Mechanical properties of specimens

All specimens were made out of the same material except column-1. Steel grade Q235 was chosen for the beam, angle and stiffeners. This research focus on the deformation of the angles, therefore a strong column was carefully chosen to remain undamaged during the test execution. The flexural deformation of the column was expected to be negligibly in all tests. Steel grade 10.9 was chosen for the high-strength friction-grip bolts. Fillet welds used between the stiffener and angle had an 8 mm leg size. The real properties of the steel were obtained by means of tensile coupon tests for every kind of steel assembly. The values obtained for the yielding stress (f_y), ultimate stress (f_u) and Young modulus (E) are summarized in Table 1.

2.4 Instrument and test procedure

The test specimens were instrumented with five dial indicators. The full instrumentation plan is described below:

1. The applied load (F) was obtained directly from the hydraulic jack read from the MTS system;

Table 1 Mechanical property of the steel parts

Items.	E (MPa)	f_y (MPa)	f_u (MPa)	$A/\%$
Column1	204981	395	590	27.3
Column2	204018	265	445	28.2
Beam	207072	250	425	29.6
Angle	203500	245	360	30.2
Stiffener	199349	320	475	29.8

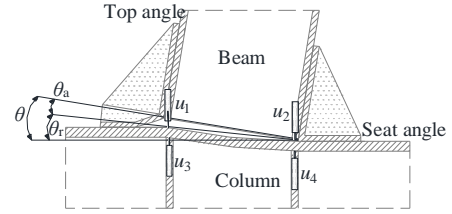


Fig. 5 Definition of the relative rotation

2. Transducer u_5 measured the total vertical displacement of the load cell near the beam end by teponosics indicator, the beam rotation can be represented by $\theta_b = u_5/l$;

3. Transducers u_1 and u_2 measured relative displacement between angle and column flange, θ_a ;

4. Transducers u_3 and u_4 were used for measuring the column shear rotation, θ_r ;

Method one:

The total rotational of the joint, θ , is the sum of the shear deformation of the column web panel zone, θ_r , and the gap rotation, θ_a , as shown in Fig. 5.

$$\theta = \theta_r + \theta_a = \frac{u_1 - u_2}{h_t} + \frac{u_3 - u_4}{h_t} \quad (1)$$

In the tests, the column was designed as a stiff part when compared to the stiffened angle shown little flexural and shear deformation. Then, θ_r is negligible; therefore, the deformation of the joint θ is equal to the beam rotation, θ_a . The measurement method is approximated by Zhan and Tao (2012).

Method two:

The total displacement obtained at the end point, u_5 caused by the joint rotation, θ , and elastic deformation of beam, θ_e . Hence the joint rotation, θ , can be evaluated by Eq. (2)

$$\theta = \theta_b - \theta_e = \frac{u_5}{l} - \frac{Fl^3}{3EI} \quad (2)$$

u_i the displacement measured by transducers, Where h_t is the vertical distance of transducers u_1 and u_2 , l is horizontal distance of the load cell and the face of the column flange. In this paper, the average value obtained by this two methods at different stages is used.

3. Finite element analysis

The numerical analysis was conducted by ABAQUS/

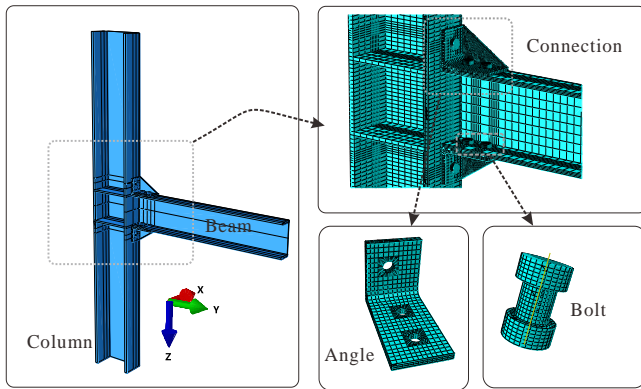


Fig. 6 Joint model and mesh of steel part

Standard (2011) module for obtaining an efficient and precise finite element method. Both material and geometry nonlinearities were considered in the analysis, the phenomenon of stiffener buckling just occurred in final phase of loading, hence a symmetrical boundary condition was considered, a half model that can reduce calculation expense was built for numerical analysis, All assembly of the numerical models are presented as follows.

3.1 Material modeling of the steel parts

The yield strength (f_y) and the ultimate strength (f_u) of the steel were adopted for every actual tensile coupon test result, as summarized earlier in Table 1. The Poisson's ratio was assumed 0.3. An isotropic hardening rule with a von Mises yielding criterion which is suitable for simulation of metal plasticity under monotonic loading was employed to simulate plastic deformations of the steel parts. A monotonic displacement history with increasing amplitude similar to the experimental loading protocol was incrementally imposed to the beam tip. For material modelling of high strength bolts, a multi-linear elastic plastic stress strain relationship was applied to the high-strength bolt constitutive model, which is usually applied for high strength steel, the ultimate strength (f_u) is 1000 Mpa and ultimate strain (ϵ_u) is 0.12 for Grade 10.9 M16 bolts, and yield strain (f_y) is 900 MPa.

3.2 Finite element model description

The connections consisted of a steel beam, column, angle, stiffeners, column stiffeners and high strength bolts. The contact, pretension, friction and real stress distribution were considered, so an 8-node linear brick incompatible mode element (C3D8I) was adopted for all parts of the specimens. The boundary conditions were in accordance with typical tests and the structured meshing technique was used to form a proper element shape, especially for round bolts and a stiffener in angle. The total meshed model and typical parts is shown in Fig. 6.

Tangent contact and normal contact were employed for the contact properties. Coulomb friction was used for tangent contact, and the friction coefficients with 0.33 were selected in terms of the tests (Citipitioglu *et al.* 2002). Hard contact was used for normal contact, which simulated the

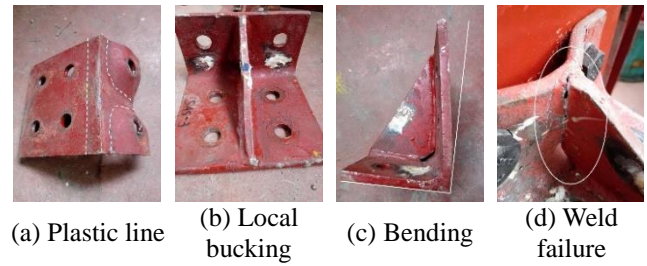


Fig. 7 Monotonic test results

extrusion phenomenon between bolts and plates. The above-mentioned methods were consistent with actual situations. A Bolt Load instruction was used for imposing pretension force in a high-strength bolt of the test. The bolts of angle connection suffered both axial force and shear force. Due to complicated contact relations and high nonlinear behaviour, the bolts and angle should be carefully meshed for acceptable convergence. Meanwhile weld in stiffened angle were modelled by the Tie option.

4. Discussing of the static experimental result

4.1 Failure mode of the angle under static loads

The column and beam were designed relative stiff to the angles, class 10.9 high-strength bolts were installed in joints. The failure mode was consistent with failure mode one in Eurocode3 part 1.8 (2005), therefore only deformation in the stiffened or unstiffened angle was of concern, the ultimate rotation (θ_{ju}) of all testing specimens were more than 0.09 rad. As illustrated in Figs. 8(a)-(h), the angles suffered the most deformation. For the type of a stiffener in tension angle (SAS-1, SAS-3), a weld failure happened between angle and stiffener. For the unstiffened type (SA-1, SAS-2), the top angle was close to be straightened, but no crack was found in the angles, the test was end due to the limit of loading device, therefore the ultimate resistance and rotation of the un-stiffened type joints were underestimated.

Specimens SAS-1 and SAS-3 had the same deformation and failure process in tension stiffened angle, it was found that angles were bended with the painting peel off after the yield, arc-shape plastic lines spread along the edge of fillet toe and welding line in the stiffened angle short leg with the increase of load, the plastic deformation was illustrated in Fig. 7(a). Along with the load increasing, a micro-crack appeared in the weld of the stiffener, finally the test was ended when the crack in tension stiffened top angle spread and resulted in a tearing of the weld as shown in Fig. 7(d). Fig. 7(b) shows some indication of the local buckling of stiffener in compression zone were observed after the test in specimens SAS-2 and SAS-3. If a thicker stiffener was adopted, this issue could be entirely avoided. Although the stiffener restricted the bending of the seat angle, obvious bending deformation had been found stiffened seat angle as shown in Fig. 7(c).

Specimens SA-1 and SAS-2 were stopped when deformation approached the limit of the loading devices, no

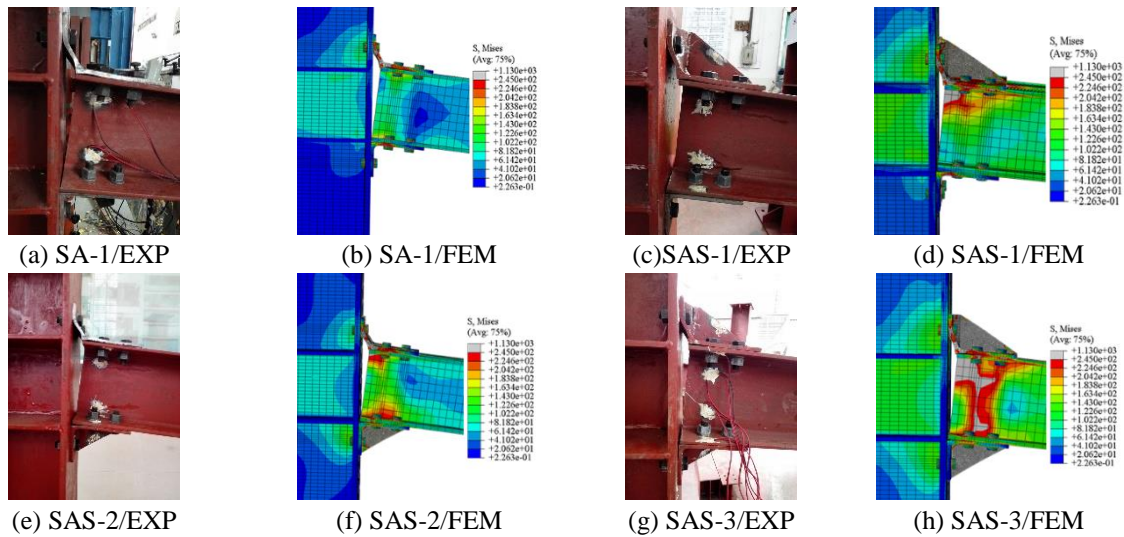


Fig. 8 Failure pattern of the experimental prediction and FEM

Table 2 Experimental initial stiffness, resistance and rotation characteristics

Items	S_{ji}	$S_{ji}'/$	S_{py}	M_p	$M_p'/$	θ_{ju}	M_u
Unit	kN.m/rad	S_{SA-1}	kN.m/rad	kN.m	M_{SA-1}	rad	kN.m
SA-1	2899	1	100.51	11.37	1	0.108	22.87
SAS-1	4866	1.68	237.81	19.09	1.68	0.089	35.45
SAS-2	3096	1.07	103.92	15.03	1.32	0.107	26.54
SAS-3	5030	1.74	288.99	23.63	2.08	0.095	45.7

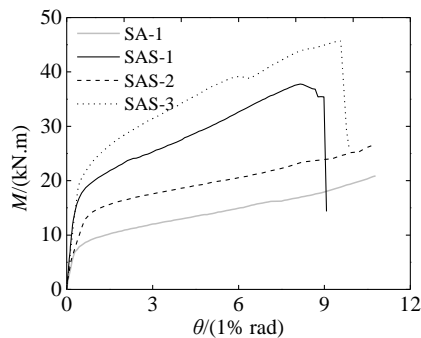


Fig. 9 Moment rotation relationship of monotonic test

crack was found in these two specimens. Meanwhile, Fig. 8(a) shows the yield lines on the top angle formed at longer leg between the first bolt row and the fillet toe were less developed than those in the shorter leg. There was no obvious deformation in the bolt shank or nut after the all test, but the washer was crushed into the bolt hole at short leg of top angle because of bolt was designed to be a stiff part relative to the angle.

4.2 Discussion on moment rotation curves of the monotonic test

The behavior of moment connections is typically represented by the $M-\theta$ curve that describes the relationship between the applied moment in connection (M) and the relative rotation between the beam and column (θ) which is described indirectly in Fig. 9.

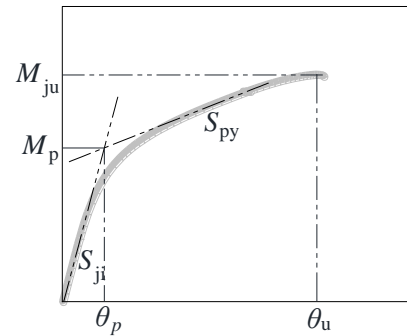


Fig. 10 Key parameter definition of monotonic test

The following characteristics are obtained from the moment rotation curves of the tests: the initial stiffness (S_{ji}), the plastic flexural resistance (M_p), the ultimate moment (M_{ju}), and the rotation (θ_{ju}) corresponding to M_{ju} . The initial stiffness (S_{ji}) is defined as the slope of linear stage of the loading and unloading branches (the unloading branch is not traced in the graphs) of the $M-\theta$ curve. The plastic flexural resistance (M_p) is given by the intersection between two tangent lines (Abidelah *et al.* 2012, Danesh *et al.* 2007): one tangent to the initial stage and the other tangent to the final stage of the $M-\theta$ curve. The first line represents the initial stiffness (S_{ji}) and the second line is on behalf of the post-limit stiffness (S_{py}). These parameters are defined in Fig. 10 and shown in Fig. 9 and Table 2.

The ratio between the plastic flexural resistance (M_p) for SAS-3 and SA-1 was $23.63/11.37=2.1$, The maximum value of the ultimate moment M_{ju} was achieved for SAS-3 with the mean value of 45.7 kN.m; This value was two times higher than group SA-1. This result indicates that the application of stiffener in tension and compression zone of connection resulted in quite higher plastic moment of resistance in comparison to un-stiffened connection. This ratio was slightly lower for SAS-1, $19.09/11.37=1.68$. SAS-2 which is the compression zone stiffened one had the lowest ratio, i.e., $15.03/11.37=1.32$; obviously the stiffener in top or seat angle can greatly enhance the plastic moment of resistance. Based on the ratios demonstrated above, the

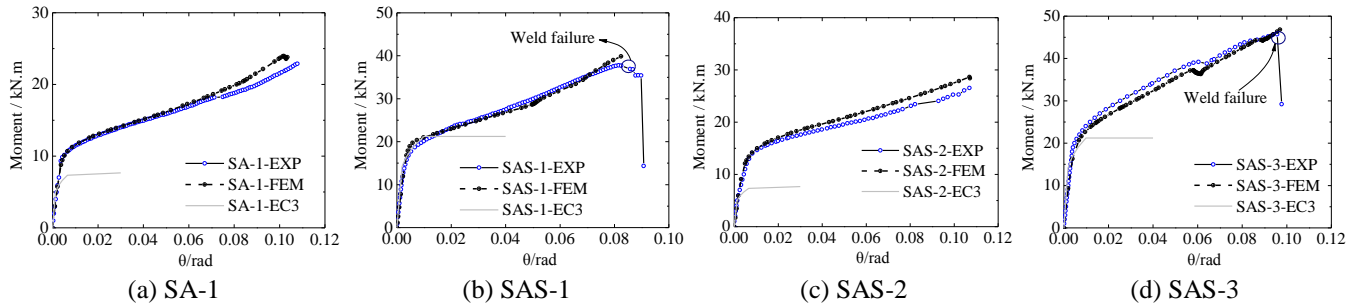


Fig. 11 Moment-rotation curves of static test

Table 3 Comparison between the experimental and analytical result

Items	S_{FE}/S_{Exp}	M_{FE}/M_{Exp}	S_{EC3}/S_{Exp}	M_{EC3}/M_{Exp}	S_{pv-FE}/S_{pv-Exp}
SA-1	0.98	0.98	1.36	0.67	1.00
SAS-1	0.95	0.88	1.55	1.11	1.20
SAS-2	1.01	1.01	1.27	0.51	1.22
SAS-3	1.02	0.96	1.49	0.90	0.98

lever arm of tension force was increased by the stiffened seat angle, while the stiffened top angle can enhance the plastic flexural resistance of this component in tension.

For the aspect of rotational stiffness, the situation was different. Especially, the initial stiffness S_{ji} was almost the same for SA-1 and SAS-2. SAS-1 was similar to the SAS-3, the highest stiffness was found in SAS-1 and SAS-3. Therefore, the stiffener in compression zone provided very little contribution to the connections initial rotational stiffness, i.e., $3096/2877=1.07$, $5030/4866=1.03$, this situation is quite different from the test result of Skejic *et al.* (2014), this phenomenon maybe be concern with the different pretension force in bolt, and the experimental result was validated by FEM simulation in follow studies, hence the experimental performance was reliable. While the stiffening of the top angle was significant, i.e., $5030/2899=1.74$. From the perspective of post limit stiffness S_{py} , the results were the same as for the initial rotational stiffness (discussed above). The minimum ratio (S_{ji}/S_{py}) acquired from the SAS-3 (17.41), while the maximum was obtained for SA-1 (28.84). Similar characteristic was found in the increment of S_{ji} and S_{py} . Eventually, in terms of the maximal reached rotation θ_{ju} , as expected the specimen SA-1 and SAS-2 had the highest value, while this value decreased when stiffener was applied in tension zone of connection with the weld failure as showed in Fig. 11.

A comparison is considered between the behavior of the connection obtained by experimental investigation and that computed by Eurocode 3 part1.8, but there is no computation guideline for the stiffened angle joint. the theoretical results refer to the stiffened column and end-plates.

According to Table 3 and Fig. 11, for the perspective of plastic flexural resistance (M_p), the response of the SA-1 and SAS-2 (un-stiffened in tension angle) that is received from experiment is significantly enhanced in comparison to the behavior computed by EC3 (2005). For the joints of stiffener in top angle, the value obtained from EC3 is close

to experimental results. The mean values of the ratio between experimental and theoretic result related to initial rotational stiffness (S_{ji}), the value obtained by EC3 is clearly overestimated.

4.3 Discussion on finite element validation

4.3.1 Finite element validation

Table 3 presents the FE analysis results in comparison with the test results. In the proposed FE model, the measured values of the yield and tensile strength were used to define the plastic behavior for all materials. As shown in Fig. 8, the results of the FE analysis agree with the experimental behavior of the examined joints. Indeed, the plastic deformation mode identified during testing corresponds to the one observed in the FE model, and the response curves show good agreement in some ways of initial rotation stiffness (S_{ji}) and plastic moment (M_p). Especially the numerical result has captured the ship occurred in test of specimen SAS-3 as shown in Fig. 11(d), this phenomenon occurred owing to the friction between steel parts was overcome. The difference between test data and numerical models grows in post limit stage, maybe a major cause is the nonlinear behavior of the steel, bolt pretensions and geometrical measuring.

A significant opening with large rotation of beam-to-column connection occurred after the test, the stiffened or un-stiffened angle suffered the highest deformation among the other part of the steel connection. According to Fig. 12 and 13, yielding expanded to the whole tension angle and stiffener in seat of compression zone at the ultimate load. This indicates that the stiffened angles are quite important for the whole behavior of connection. For this reason, the following FEM study will further discuss how it affects the response of the structure by conducting a parametric investigation.

4.3.2 Response of the stiffened angles

In FE models, the stiffened and un-stiffened angles suffer the maximum deformation among the other steel parts. At the ultimate state, the stiffener is almost completely yielding in Fig. 12(a). Fig. 12(b) show the PEEQ (equivalent plastic strain) in stiffened angle, a vertical and a horizon plastic line form around the bolt hole duo to the strong constraint by high-strength bolt, another two plastic lines that develop along the fillet and weld are more obvious. This phenomenon means that the stiffener

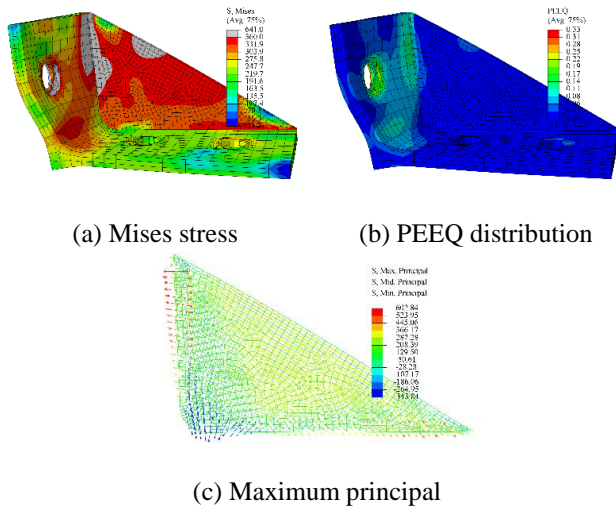


Fig. 12 Geometry configuration of steel specimens

Table 4 Parameter study results of the influence of a stiffener in seat angle

Specimens	S_{ji} kN.m/rad	$S_{ji}/S_{ji-R-SA-1}$	M_p kN.m	$M_p/M_{p-R-SA-1}$
R-SA-1	3421	1.00	10.99	1.00
R-SAS-1	6320	1.85	18.09	1.65
R-SAS-2	3518	1.03	14.17	1.29
R-SAS-3	6450	1.89	21.82	1.99
R-SAS-2-tie	4012	1.17	14.7	1.34
R-SAS-3-tie	6962	2.04	21.88	1.99

and long leg of angle show similar constraint in comparison with the bolt. The stiffened angle deformed as a 1/4 simple supported plate under concentrate load. As expected, the maximum value PEEQ that locates at bolt hole equal to 0.33.

Adding stiffeners in angle can change the loading transmit path, the shear force was more inclined to transfer from stiffener, principal stress distribution is illustrated in Fig. 12(c), the maximum principal stress is marked by red line, upper weld edge of stiffener is suffered about 602.84 MPa that is beyond the ultimate tension resistance of the weld, therefore the numerical simulation has captured the failure reason of weld and more attention should be paid in welding on stiffeners in engineering design and practice.

In order to assess the influence of stiffened seat angle on initial stiffness and plastic moment resistance, a modified model which eliminate the influence of column was selected to carry out parameter study, the column was set as a rigid part in numerical analysis. The difference of the six models lies in the arrangement of stiffener base on SAS-3. Details and results of the models were listed in Table 4. According to the comparison between R-SA-1 and R-SAS-2, R-SAS-1 and R-SAS-3, the initial stiffness (S_{ji}) was not affected by adding stiffener in seat angle, but stiffened seat angle can improve plastic moment resistance (M_p). To explain this phenomenon, R-SAS-2-tie and R-SAS-3-tie were built and modeled that Tie constraint was used in the surfaces between seat angle flange leg and beam flange, a strong constraint as weld was established similar to

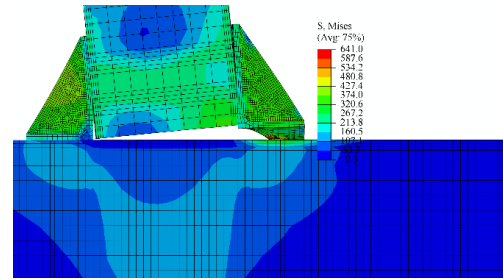


Fig. 13 Deformation of the connection in finite element analysis

Table 5 Comparison between the experimental and analytical result

Items	M_y Unit	θ_y mrad	M_{max} kN.m	θ_{max} mrad	θ_u mrad	μ_θ
CSA-1	14.37	7.6	17.77	89	89	11.71
CSAS-3	30.14	7.7	34.49	49	66	8.57
CWAS-3	29.67	11.0	35.46	49	63	5.73
CSAS-4	34.43	7.0	40.43	40	60	8.57

situation of stiffened extended end-plate connection, Under these circumstances, S_{ji} increased, meanwhile M_p was the same as the none tie one as shown in Table 4. It means that the bolt can't completely restrict the opening of the interfaces at initial loading, therefore the initial rotation center is around the interface as shown in Fig. 13, as the load increased, the stiffener started to restrict the bending of seat angle, this additional effect increase the lever arm between tension forces and compression forces when the connection achieves the plastic moment.

5 Discussing of the cyclic experimental result

5.1 General behaviour

The Table 5 summarizes most primary test results and key parameters represented the behavior of cyclic loading specimens. The plastic flexural strength of the beam, M_{pb} , for all specimens were calculated based on actual material tensile coupon tests. The test moment was computed by multiplying the force at load jack with the distance between the beam tip and the outside face of the column flange. All specimens performed well with good ductility, and the plastic deformation were formed in the unstiffened and stiffened angle. According to the transducers u_3 and u_4 , none inelastic deformation was discovered in the column throughout the test. The vertical shaft of hysteresis curve represents the ratio of applied moment, M , between the beam section of plastic bending moment, M_{pb} , to facilitate unified processing data. Fig. 18 shows the process of the hysteresis curve when the connection maximum resistance was decreased to about $M_d=85\%M_{max}$ (Park and Paulay 1975). As a matter of fact that the joints were loaded to 40% M_u , in accordance with SAC Joint Venture (1997) or to cracking. The rotation (θ_d) corresponding to M_d for all specimens were greater than 0.04 rad, the rotation capacities of the specimens satisfied the ductility requirement because

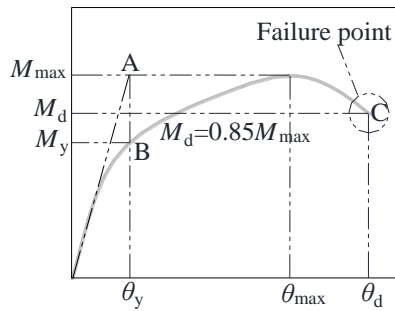


Fig. 14 Definition of a hysteretic loop by R. Park method



(a) CSA-1 (b) CWAS-3 (c) CSAS-3 (d) CSAS-4

Fig. 15 Failure modes of cyclic specimens

they had no less than 0.03 radians for earthquake resistance, as suggested by FEMA-350 (2000).

5.2 Failure mode of the cyclic test

The responses of specimens CSA-1 are shown in Fig. 19(a). Initial yielding occurred during cycle 7 with 5 mrad rotation in the short angle legs. Upon progressing through the loading history, complete fracture suddenly occurred at the long leg of seat angle with 0.09rad. Then, the applied load dropped below 40% M_{max} . CWAS-3, CSAS-4 and CSAS-4 showed good energy absorption with no slip during the loading history. Strength and stiffness degradation was not obvious at the same load level before the connection cracked. The failure process of three specimens were similar. Initial yielding was found at the short angle legs. Then, with an increase of loads, the short angle leg split away from the connected column flange. Meanwhile, an arc-shaped yield line appeared with flaking paint as the monotonic experiment. Subsequently a micro-crack appeared in the short tension angle leg near the weld after the drift achieved 0.04 rad at the first lap in CSAS-4. Then, a small crack spread to the toe of the top short angle leg of specimen CSAS-4 that resulted in the drop of the ultimate bending resistance. While strength of CWAS-3 and CSAS-3 continued to rise at the drift of 0.05 rad, even with a small crack. Then, the specimens tore apart by step as shown in Fig. 16, when the rotation increased. The failure process of CWAS-3 is shown in Fig. 13. The final state of all cyclic test specimens is seen in Fig. 14. Fig. 12 illustrates the cyclic loading strength degeneration. CSAS-4 reached M_{max} at the drift of 0.04 rad. CWAS-3 and CSAS-4 attained M_{max} at the drift of 0.05 rad. As the increase of the rotation, the strength of specimens didn't suddenly dropped to a relative low value, when the rotation of the three specimens reached 0.08 rad, the joints could bear a load above 50% M_{max} . Therefore, the test stiffened angle

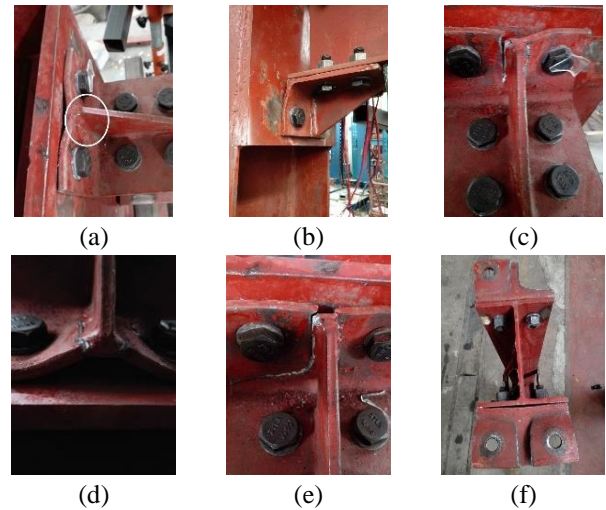


Fig. 16 Joints failure process

connection has a certain degree of redundancy. This feature has potential in application of post-tension system.

5.3 Moment rotation curves and skeleton curves

The skeleton curve reflects the relationship between the M and θ of the specimen under cyclic loading. It is obtained by connecting the peak value point of every cycle loop (unloading point). The main properties of the M and θ curves of cyclic test is shown in Table 5. In comparison with specimen CSA-1, the ultimate moment and maximum moment of all stiffened specimens increased above 110%. The θ_{max} declined from 0.089 rad to 0.049 rad for specimens CWAS-3 and CSAS-3. The ultimate rotation declined to 0.04rad for specimen CSAS-4. Therefore, the result indicated that stiffener in angle significantly improved its resistance but reduces its ultimate rotation. Compared with CSAS-3, the CWAS-3 (column flange welding plate connections of weak axis) exhibited similar properties in terms of the plastic moment M_p , ultimate moment M_u and ultimate rotation θ_u . This new type angle connection has showed good rotation and processed certain stiffness and strength could be utilized in minor axis joints. The connection plate which was welded to the edge of column flange could be considered as a stiffening part of column in major axis. The space between stiffeners in minor axis and column web has potential for satisfying architectural requirements such as ducting (Tagawa and Liu 2014). CSAS-4 is top-and-seat angle connection with double web angle stiffened with stiffeners, in comparison with CSAS-3, its ultimate capacity was increased by 14%, but maximum rotation dropped 0.009 rad.

5.4 Ductility

Inter-story drift capacity and ductility ratio are used to describe the ductility of the four specimens. According to AISC (2010), the inter-story drift capacity is defined as the drift corresponding to the beam tip load degrading to 0.8 of the peak load, and joints with inter-story drift. Joints with inter-story drift capacities no less than 0.04 rad are believed

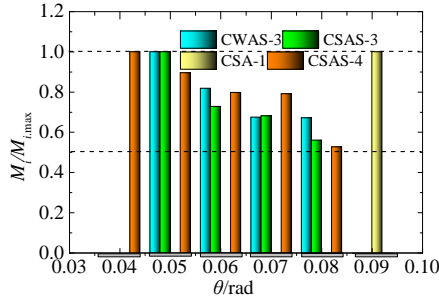


Fig. 17 Cyclic loading strength variation

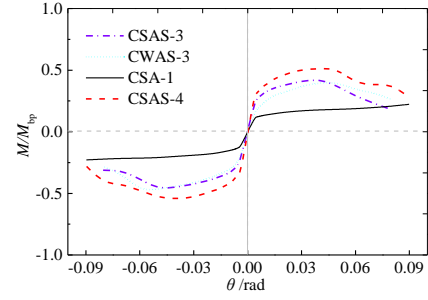
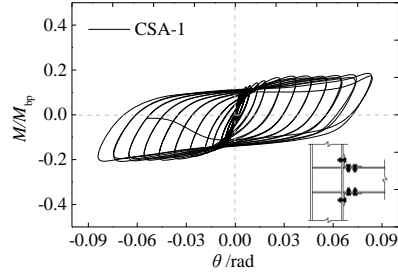
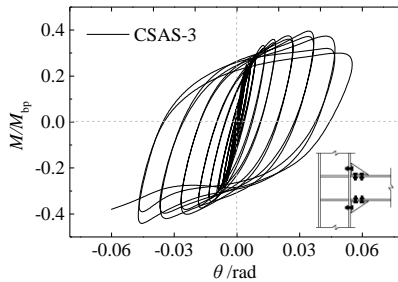


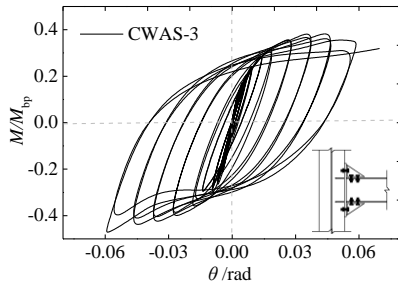
Fig. 19 Skeleton curves



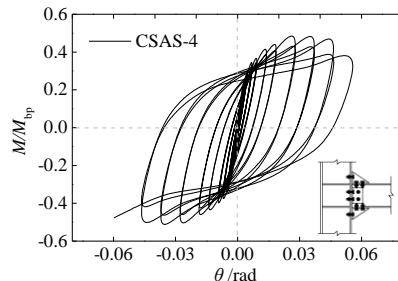
(a) CSA-1



(b) CSAS-3



(c) CWAS-3



(d) CSAS-4

Fig. 18 Hysteretic curves

to have sufficient ductility under seismic actions for special moment frames. The inter-story drift was taken as Δ/L ratio in this study (where Δ =beam tip displacement, L =length of

lever arm), and the ductility ratio was defined using Eq. (3)

$$\mu_{\theta} = \theta_y / \theta_d \quad (3)$$

where, according to the Park and Pailay (1975) as shown in Fig. 14, θ_d is the drift corresponding to the ‘failure point’ C (where beam tip load degraded to 85% of the peak load), and θ_y is the drift corresponding to the ‘yield point’ B. The yield point B is the intersection point of a vertical line and the M - θ curve. As expected, the magnitude of μ_{θ} was decreased with stiffeners, however, the reduction isn’t high for specimen CSAS-3 and CSAS-4.

5.5 Energy absorption

The energy absorption is important in seismic activity, and the total dissipative energy is defined as the area of hysteretic curves, which indicates the energy dissipation capacity. Equivalent viscous damping (EVD) is one of the three key parameters expressing the energy dissipation capacity of connection component. The method to calculate EVD as defined in Fig. 20 (Tong *et al.* 2016). In Eq. (4), S_{ABC} and S_{CDA} refer to the upper half and lower half areas of the hysteretic curve, respectively. S_{OBE} and S_{ODF} represent corresponding triangular areas.

$$h_e = \frac{1}{2\pi} \frac{S_{ABC} + S_{CDA}}{S_{OBE} + S_{ODF}} \quad (4)$$

Fig. 21 describes the changes of EVDs of the four specimens with increasing inter-story drift. As pointed out in Fig. 21, at the drift level of 0.04 rad, the values of EVD for all tested cyclic specimen were above 0.25, which indicates good energy dissipation capacity of all specimens.

Another two properties, namely, energy dissipated in each steps (E_i), accumulated energy dissipation (E_t). Fig. 22(a)-(b) shows the E_i and E_t of the four specimens, The accumulated energy dissipations of the specimens at failure varied between 24 kJ to 45 kJ. For the three specimens with stiffeners show similar responses at ultimate state, the E_t of specimen CSAS-4 at 0.04 rad was almost triple that specimen CSA-1 and 1.14 times CSAS-3, therefore, the presence of double stiffener could highly enhanced energy dissipation behavior, however, in comparison of CSAS-3 and CSAS-4, the increasing caused by double web angles isn’t obvious when compared to the stiffeners. It’s worth noting that the overall performance of specimen CWAS-3 (the minor axis joint) was worse than other two stiffened types.

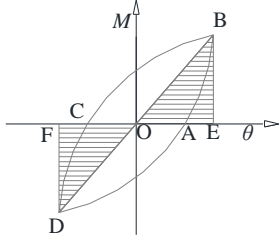


Fig. 20 Definition of a hysteretic loop

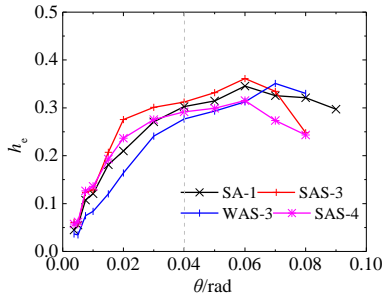
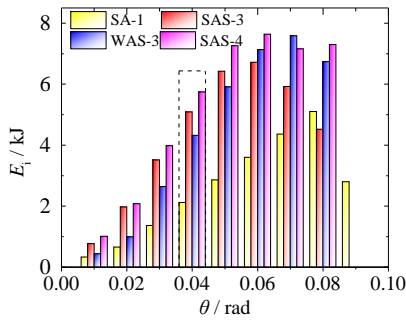
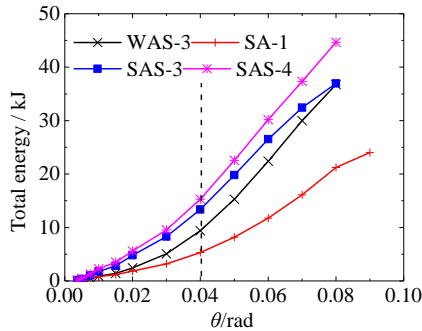


Fig. 21 Equivalent viscous damping



(a) Energy dissipated during in each step



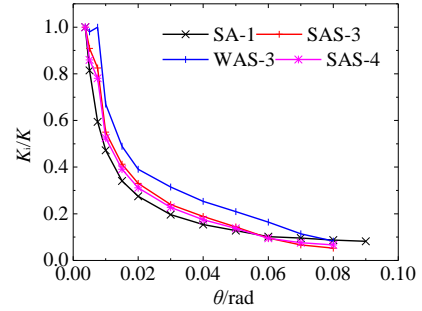
(b) Accumulated energy dissipation

Fig. 22 Energy dissipation capacity

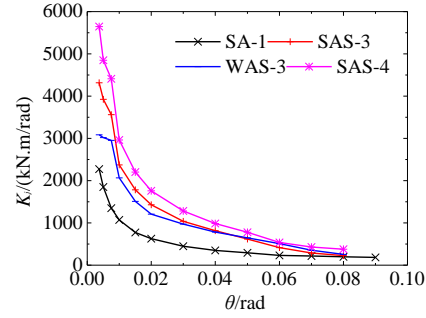
The change of the secant stiffness of the joints with increasing number of cycles can be illustrated through the K/K_i ratio, where K is the secant stiffness of the joint in the considered cycle, and K_i is that in the initial cycle. The secant stiffness K is defined by Eq. (2)

$$K = \frac{M_B - M_D}{\theta_B - \theta_D} \quad (5)$$

The stiffness degradation is shown in Fig. 23. Respectively, a similar trend of specimens CSA-1, CSAS-3 and CSAS-4 was found in stiffness degradation, the initial

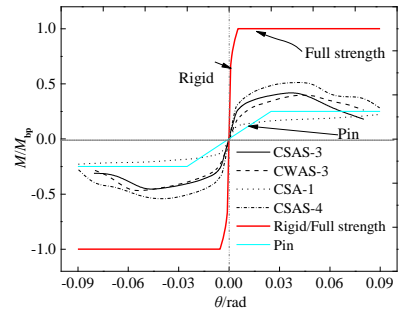


(a)

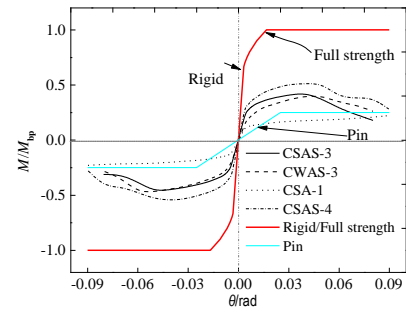


(b)

Fig. 23 Stiffness degradation curves



(a) Braced frame



(b) None braced frame

Fig. 24 Classification of tested joints

stiffness of specimen WAS-3 was less than CSAS-3 due to out of plane stiffness of welding plate, moreover, stiffness degradation is more slowly than other three specimens. In addition, the stiffeners were more effective than double web angles in increasing initial rotation stiffness.

5.6 Classification by rigidity and strength

A connection could normally be classified as nominally

pinned, semi-rigid or rigid in terms of stiffness as recommended by EC3 (2005). A joint is nominally pinned when the initial rotational stiffness is less than $0.5 EI/L$, where E , I and L are elasticity modulus, second moment of area, and the length of the steel beam, respectively. A rigid joint is that with the initial rotational stiffness greater than $25 EI/L$ for non-braced frame and $8 EI/L$ for braced frame. For the perspective of strength, the minimum required connection resistance for partial-strength design is $0.25 M_{pp}$, the full strength connection resistance is beyond M_{pp} . According to the $M-\theta$ hysteretic curves in Fig. 19, the boundary of rigid, pin and strength are calculated and illustrated in Fig. 24. This indicates that the considered stiffened specimens were semi-rigid and partial-strength joints.

6. Conclusions

This paper has described monotonic and cyclic tests of top-and-seat angle connection with stiffeners. Finite element analysis was used to validation and parameter study, the following observations and conclusions can be drawn.

- 1) Three types stiffened angle joints can be classified as semi-rigid and partial strength by EC3 specification.
- 2) When the joints are subjected to negative moment, the plastic flexural resistance and initial rotational stiffness of nominally identical connections can be remarkably enhanced by adding stiffener in the top angle; however, experimental results and finite element parameter study show that adding stiffener in the seat angle had little effect on the initial rotational stiffness due to weak constraint provided by bolts at initial stage. However, it can increase the plastic flexural resistance of the connection.
- 3) The failure mechanism of stiffened angle connections under monotonic and cyclic loads was different, the weld was torn apart for monotonic loads but arc-shaped plastic fracture was found in cyclic test. The numerical simulation results show that welds around upper stiffener has the highest Mises stress. Therefore the numerical simulation has captured the failure reason of weld and more attention should be paid in welding of stiffener in engineering design and practice.
- 4) When the three stiffened cyclic specimens reached 0.08 rad, the joints could bear a load above 50% M_{max} , the connection has certain robustness.
- 5) A stiffener in angle significantly improves its ultimate resistance but reduces its ultimate rotation, especially for stiffened angle connection with double web angles. For all stiffened angle connections, the ultimate rotation was greater than 0.04 rad, which satisfies the ductility requirement of no less than 0.03rad for earthquake resistance suggested by FEMA-350.
- 6) According to cyclic testing, adding stiffeners in top-and-seat angle is a more effective way than adding double web angles to enhanced accumulated energy dissipation and initial rotational stiffness, in addition, the index of ductility was slightly reduced.

Acknowledgments

This study was supported by National Natural Science Foundation of China (Grant No. 51778241; 51708226; 51378009; 51378219; 51638009) and by State Key Laboratory of Subtropical Building Science of South China University of Technology (Grant No.2018ZB35, 2017ZB28, and 2017KD22) and by the Fundamental Research Funds for the Central Universities (Grant No. 2017BQ086; 2017ZD026).

References

- ABAQUS Analysis User's Manual (2011), *ABAQUS Standard*, Version 6.10
- Abdalla, K.M., Drosopoulos, G.A. and Stavroulakis, G.E. (2014), "Failure behavior of a top and seat angle bolted steel connection with double web angles", *J. Struct. Eng.*, **141**(7), 04014172.
- Abidelah, A., Bouchair, A. and Kerdal, D.E. (2012), "Experimental and analytical behavior of bolted end-plate connections with or without stiffeners", *J. Constr. Steel Res.*, **76**(3), 13-27.
- AISC (1995), Manual of Steel Construction-load and Resistance Factor Design, American Institute of Steel Construction, Chicago, IL, USA.
- Akiyama, H. (2000), "Evaluation of fractural mode of failure in steel structures following Kobe lessons", *J. Constr. Steel Res.*, **55**(1-3), 211-227.
- ANSI/AISC 341-10 (2010), An American National Standard, Specification for Structural Steel Buildings, American Institute of Steel Construction, Chicago, USA.
- Aydin, A.C., Kilic, M., Maali, M. and Sagiroglu, M. (2015), "Experimental assessment of the semi-rigid connections behavior with angles and stiffeners", *J. Constr. Steel Res.*, **114**, 338-348.
- Azizinamini, A. and Radziminski, J.B. (1989), "Static and cyclic performance of semirigid steel beam-to-column connections", *J. Struct. Eng.*, **115**(12), 2979-2999.
- Brunesi, E., Nascimbene, R. and Rassati, G.A. (2014), "Response of partially-restrained bolted beam-to-column connections under cyclic loads", *J. Constr. Steel Res.*, **97**, 24-38.
- Citipitioglu, A., Rami Hajali, M. and White, D.W. (2002), "Refined 3D finite element modeling of partially-restrained connections including slip", *J. Constr. Steel Res.*, **58**(5-8), 995-1013.
- Danesh, F., Pirmoz, A. and Daryan, A.S. (2007), "Effect of shear force on the initial stiffness of top and seat angle connections with double web angles", *J. Constr. Steel Res.*, **63**(9), 1208-1218.
- Eurocode 3 (2005), Design of Steel Structures, Part 1-8: Design of Joints, European Committee for Standardization, EN 1993-1-8, Brussels
- Faella, C., Piluso, V. and Rizzano, G. (1999), *Structural Steel Semirigid Connections: Theory, Design and Software*, CRC Press, Italy
- Feizi, M.G., Mojtahedi, A. and Nourani, V. (2015), "Effect of semi-rigid connections in improvement of seismic performance of steel moment-resisting frames", *Steel Compos. Struct.*, **19**(2), 467-484.
- FEMA-350 (2000), Recommended Seismic Design Criteria for New Steel Moment-Frame Buildings, Federal Emergency Management Agency, Rep. FEMA-350, Washington D.C., USA.
- Garlock, M.M., Ricles, J.M. and Sause, R. (2003), "Cyclic load tests and analysis of bolted top-and-seat angle connections", *J.*

- Struct. Eng.*, **129**(12), 1615-1625.
- GB50017-2003 (2003), Code for Design of Steel Structures, Ministry of Construction of the PRC, Beijing, China.
- Ghassemieh, M., Shamim, I. and Gholampour, A.A. (2014), "Influence of the axial force on the behavior of endplate moment connections", *Struct. Eng. Mech.*, **49**(49), 23-40.
- Guo, B., Gu, Q. and Liu, F. (2006), "Experimental behavior of stiffened and unstiffened end-plate connections under cyclic loading", *J. Struct. Eng.*, **132**(9), 1352-1357.
- Kukreti, A.R. and Abolmaali, A. (1999), "Moment-rotation hysteresis behavior of top and seat angle steel frame connections", *J. Struct. Eng.*, **125**(8), 810-820.
- Liu, Y., Malaga-Chuquitaype, C. and Elghazouli, A.Y. (2014), "Behaviour of open beam-to-tubular column angle connections under combined loading conditions", *Steel Compos. Struct.*, **16**(2), 157-185.
- Mahin, S.A. (1998), "Lessons from damage to steel buildings during the Northridge earthquake", *Eng. Struct.*, **20**(4-6), 261-270.
- Park, R. and Paulay, T. (1975), *Reinforced Concrete Structures*, John Wiley and Sons Inc., New York.
- Piluso, V. and Faella, C. (1998), "Experimental analysis of bolted connections: Snug versus", *J. Struct. Eng.*, **124**(7), 765-774.
- Reinosa, J.M., Loureiro, A., Gutierrez, R. and Lopez, M. (2015), "Analytical plate approach for the axial stiffness prediction of stiffened angle cleats", *J. Constr. Steel Res.*, **106**(106), 77-88.
- Shi, G., Shi, Y. and Wang, Y. (2008), "Behaviour of end-plate moment connections under earthquake loading", *Eng. Struct.*, **29**(5), 703-716.
- Shiravand, M.R. and Mahboubi, S. (2016), "Behavior of post-tensioned connections with stiffened angles under cyclic loading", *J. Constr. Steel Res.*, **116**, 183-192.
- Skejić, D., Dujmović, D. and Beg, D. (2014), "Behaviour of stiffened flange cleat joints", *J. Constr. Steel Res.*, **103**(12), 61-76.
- Tagawa, H. and Liu, Y. (2014), "Stiffening of bolted end-plate connections with steel member assemblies", *J. Constr. Steel Res.*, **103**, 190-199.
- Tong, L., Chen, Y., Chen, Y. and Fang, C. (2016), "Cyclic behaviour of beam-to-column joints with cast steel connectors", *J. Constr. Steel Res.*, **116**, 114-130.
- Venture, S.J. (1997), "Protocol for fabrication, inspection, testing, and documentation of beam-column connection tests and other experimental specimens", Report no. SAC/BD-97/02, SAC Joint Venture, Sacramento, California, USA.
- Zhan, W. and Tao, W. (2012), "Experiment and finite element analysis for the end plate minor axis connection of semi-rigid steel frames", *China Civil Eng. J.*, **45**(8), 83-89.